FULL PAPER

ADVANCED FUNCTIONAL MATERIALS

DOI: 10.1002/adfm.200700222

# High-Efficiency Red Phosphorescent Iridium Dendrimers with Charge-Transporting Dendrons: Synthesis and Electroluminescent Properties

By *Bo Liang*, *Lei Wang*, *Yunhua Xu*, *Huahong Shi*, and *Yong Cao**

A series of 1-phenylisoquinoline derivatives encapsulated with peripheral arylamines as dendrons are synthesized by using the Ullmann reaction and palladium-catalyzed aromatic carbon–carbon Suzuki-coupling reactions. Red-emitting dendritic iridium complexes (called **G1-1**, **G1-2**, and **G2**) are synthesized using the following derivatives: *N*,*N*-diphenyl-3′-isoquinolin-4-biphenylaniline, *N*,*N*-di(9,9-dimethylfluorenyl-3′-isoquinolin-4-biphenylaniline, *N*,*N*-di(4′-di(2′-(9′,9′-dimethylfluorenyl)amine)biphenyl-3′-isoquinolin-4-biphenylaniline as the first ligands and 5-methyl-3-(pyridin-2′-yl)-1H-1,2,4-triazole as an ancillary ligand. The obtained dendrimers are soluble in common organic solvents, and uniform thin films can be spin-coated from such solutions. Devices fabricated from dendritic iridium complexes **G1-2** and **G2** with a small molecule host are fabricated by spin-coating from chloroform solution in different device configurations. **G1-2** and **G2** show similar device performances with maximum external quantum efficiencies (EQEs) of 12.8 % and 11.8 % (photons/electron) and luminous efficiency of 9.2 cd $A^{-1}$ and 8.5 cd $A^{-1}$ at 0.1 mA $cm^{-2}$, respectively. Devices based on polymer host poly(9,9-dioctylfluorene)(PFO) (30 % PBD (2-(4-biphenyl)-5-(4-tert-butylphenyl-1,3,4-oxadiazole)) show a slightly higher efficiency for **G1-2**, with a maximum EQE of 13.9 % at a much higher current density of 6.4 mA $cm^{-2}$ and luminance of 601 cd $m^{-2}$.

## 1. Introduction

Organic light-emitting diodes (OLEDs) have attracted considerable attention during recent years in the fields of academic research and display technology.[1] The development of high-performance materials is of key importance for the fabrication of high-performance OLEDs. Ir complexes have been investigated extensively as phosphorescent emitters because of their high efficiency, (potentially 100 % for internal quantum efficiency), and tunable emission color in the whole visible region via ligand modification.[2] Devices have typically been made from Ir(III) complexes doped into wide-band-gap small molecule hosts deposited under high vacuum by using thermal evaporation.[3] In recent years, a new class of functional organic material, dendrimers, have been developed as a new kind of electroluminescent material.[4–6] The dendritic structure allows independent modification of the core (light emission), branching groups (charge transport), and surface groups (processing properties). Phosphorescent dendrimers have either homoleptic or heteroleptic Ir complexes as a luminescent core onto which dendrons are attached. The surface groups and dendrons provide processing flexibility and transport properties, and also modify intermolecular interactions of the light-emitting cores. Phosphorescent dendrimers are attractive as light-emitting materials because they can combine high efficiency, good color-tunability, and solution processability of the active layers, as can polymer LEDs. Furthermore, phosphorescent cores are separated by bulky dendrons so triplet–triplet (T–T) annihilations of the complexes can be efficiently suppressed. High-efficiency green-emitting dendrimer devices of 55 cd $A^{-1}$ (40 lm $W^{-1}$) at 4.5 V (400 cd $m^{-2}$) for two-layer devices[7] and 12.8 lm $W^{-1}$ at 8.1 V (550 cd $m^{-2}$) for single layer[8] devices have been reported. The green-emitting device fabricated with a second-generation Ir dendrimer with rigid hole-transporting carbazole dendrons realized a maximum external quantum efficiency (EQE) of 16.6 % when doped into 4,4′-bis(N-carbazolyl)biphenyl (CBP).[9] There are few papers reporting red-emitting phosphorescent dendrimers: of them the highest device efficiency, reported by Anthopoulos et al.[10] was only 5.7 % at 80 cd $m^{-2}$ and 5 V for a bilayer device structure, much lower than that for green dendrimer devices or thermally deposited small-molecule red phosphorescent OLEDs (PhOLEDs).

Aryl-substituted quinolines are a class of cyclometallated ligands that are well-suited for use as high-efficiency red electro-

[*] Prof. Y. Cao, Dr. B. Liang, L. Wang, Y. H. Xu, Dr. H H. Shi
Institute of Polymer Optoelectronic Materials and Devices
Key Laboratory of Specially Functional Materials
South China University of Technology
Guangzhou 510640, P.R. China
E-mail: poycao@scut.edu.cn

[**] The authors are deeply grateful to the National Natural Science Foundation of China (Project No. 50433030) and the MOST National Research Project (No. 2002CB613403) for their financial support. Supporting Information is available online from Wiley InterScience or from the author.

ADVANCED FUNCTIONAL MATERIALS



phosphorescent homoleptic and heteroleptic Ir complexes.[11] Tsuboyama et al.[12] reported that tris(1-phenylisoquinolinato-*C*2,*N*)iridium(III) ($Ir(piq)_3$), a phosphorescent dopant, achieved a high efficiency, that is, an EQE $\eta_{ext} = 10.3\,\%$ and power efficiency of 8.0 lm $W^{-1}$, at 100 cd $m^{-2}$. Duan et al.[13] reported a device based on (2-methyldibenzo[f,h]quinoxalino(*C*2,*N*′)) iridium(III) acetylacetonate ($Ir(MDQ)_2acac$) with a high EQE of 12.4 %, brightness of 58 160 cd $m^{-2}$ and current and power efficiency respectively of 26.2 cd $A^{-1}$ and 13.7 lm $W^{-1}$ with the following device structure: NPB (4,4′-bis[*N*-(I-napthyl)-*N*-(pherylamino)-biphenyl) (50 nm)/Ir(MDQ)$_2$acac: CBP (5.7 %, 30 nm)/TPBI (15 nm)/Alq (35 nm) (TBPI = 1,3,5-tris(2-*N*-phenylbenzimidazolyl)benzene). The heteroleptic complexes have two cyclometalated ligands and an ancillary ligand. The emitting color from the Ir complex is dependent on the choice of both the cyclometalated and ancillary ligands. Synthesis of homoleptic complexes such as tris(2-phenylpyridine) iridium ($Ir(ppy)_3$) proceeds at high temperature and requires a longer reaction time.[12,14a] Heteroleptic cyclometalated Ir complexes are typically prepared via addition of a third ligand to the Ir dichloroprecursor and the reaction proceeds at a much lower reaction temperature with relatively high yields.[14b]

In this paper, we report the synthesis and properties of a novel class of high-performance red-emitting Ir dendrimers. The dendrimers were modified with first- and second-generation triarylamine as cyclometalated ligands and a triazole compound as the ancillary ligand. The obtained dendrimers were fully characterized. By spin-coating the dendrimers doped into small molecule or polymer hosts from chloroform solution, a series of high-efficiency double-layer light-emitting devices were obtained. Our research revealed that the variation of the $\pi$-conjugation length of the triarylamine unit optimized the hole-transporting ability, and that the fluorenyl-substituted triarylamine on the surface led to the separation of the light-emitting core, thus reducing the aggregation and providing good solubility.

## 2. Results and Discussion

### 2.1. Synthesis

Syntheses of ligands and Ir dendrimers are shown in Schemes 1 and 2, respectively. The ligands 1-phenylisoquinoline (1-piq)[15] and 5-methyl-3-(pyridin-2′-yl)-1H-1,2,4-triazole (mpt; **13**)[16] are synthesized according to the literature; **8** is synthesized according to a procedure reported in Doi et al.[17] The first (**G1-1**, and **G1-2**) and second-generation (**G2**) ligands are synthesized by using the modified Ullmann reaction and Suzuki-coupling reaction,[18] respectively. These ligands based on 1-piq are used as core, and triarylamine groups are used as dendrons. The heteroleptic complexes are prepared according to a two-step method reported in the literature.[19] Ir dimers are synthesized first and then reacted with 3–5 times an equivalent amount of **13** and an equivalent amount of sodium methoxide in ethanol at 50 °C for 3–5 h. All experiments involving Ir(III)

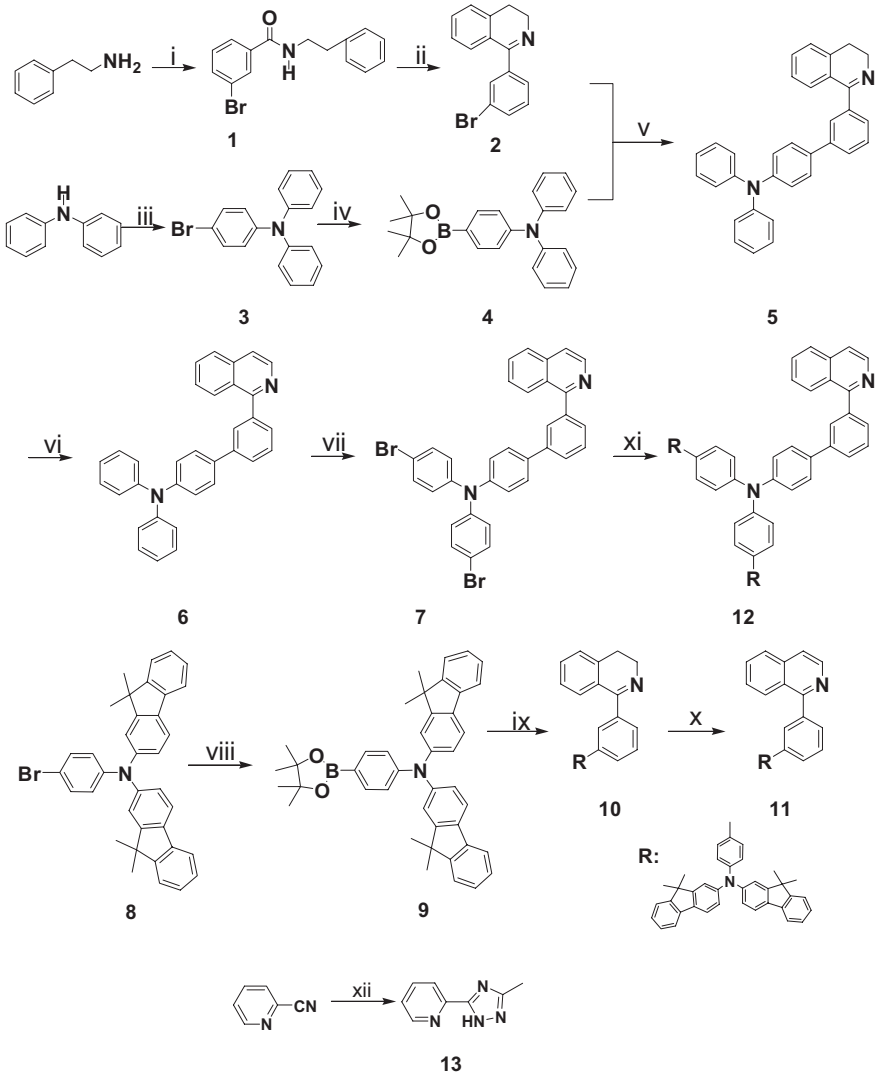


**Scheme 1.** Synthetic route for the ligands. Reagents and conditions: i) 3-bromobenzoyl chloride, $Et_3N$, $CH_2Cl_2$, room temperature (RT), 4 h; ii) xylene, $P_2O_5$, $POCl_3$, refluxed 3 h; iii) 4-bromoiodobenzene, 1,10-phenanthroline, CuCl, anhydrous KOH, xylene, Ar, refluxed, 24 h; iv) THF, *n*-BuLi, –78 °C, 2-isopropoxy-4,4,5,5-tetramethyl-1,3,2-dioxaborolane, then to RT, 24 h; v) $Pd(PPh_3)_4$, $Na_2CO_3$, toluene/ethanol = 2:1, 100 °C, Ar, 24 h; vi) 10 % Pd/C, mesitylene, 190 °C, Ar, refluxed 3 h, vii) NBS (*N*-bromosuccinimide), $CHCl_3$, RT, 5 h; viii) THF, *n*-BuLi, –78 °C, 2-isopropoxy-4,4,5,5-tetramethyl-1,3,2-dioxaborolane; ix) $Pd(PPh_3)_4$, 2 M $Na_2CO_3$ solution, toluene/ethanol = 2:1, 100 °C, Ar, 24 h; x) 10 % Pd/C, mesitylene, 190 °C, Ar, refluxed 3 h, xi) $Pd(PPh_3)_4$, $Na_2CO_3$, toluene/ethanol = 2:1, 100 °C, Ar, 24 h. xii) $NH_2NH_2.H_2O$, refluxed, 3 h, $CH_3COOH$, 3 h.

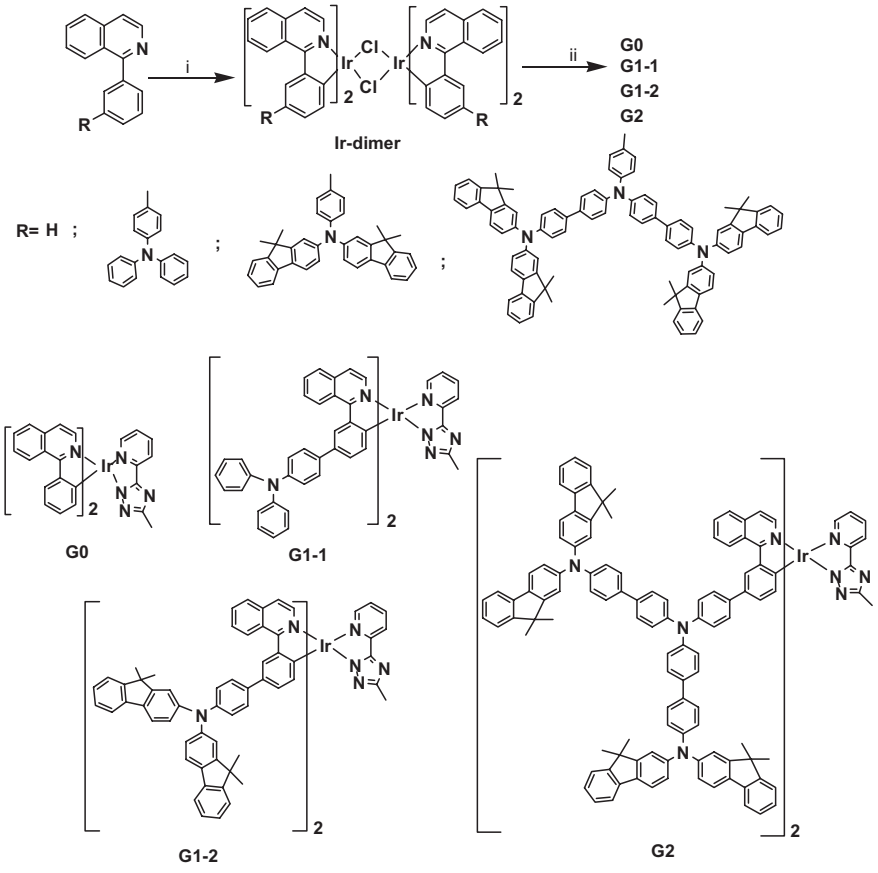


**Scheme 2.** Synthetic route for the Ir-complex dendrimers. Reagents and conditions: i) $IrCl_3.3H_2O$, 2-ethoxylethanol/$H_2O$ (3:1), 120 °C; ii) $NaOCH_3$, ethanol, 50 °C, **13**, refluxed 3–5 h.

species were carried out in an inert atmosphere, despite the good stability of the compounds in air. The main concern is the oxidative and thermal stability of intermediate complexes at the high temperatures reached during the reaction.

All the dendritic Ir complexes have good solubility in common organic solvents, such as chloroform, acetone, and chlorobenzene, and it is easy to form a uniform film from them by using spin-coating. The structures of these compounds were verified by using $^1$H NMR spectroscopy. The molecular weights were tested by using gas-chromatography mass spectrometry (GC-MS), electrospray-ionization mass spectroscopy (ESI-MS), or matrix-assisted laser desorption–ionization time-of-flight (MALDI-TOF) mass spectrometry. The ESI-MS of Ir complexes (**G0**, **G1-1**, and **G1-2**) showed a molecular-weight peak, corresponding to $MH^+$(100 %), and a weaker peak, attributed to the fragment of $[MH-160]^+$ with a molecular weight ($M_{wmpt}$) of 160*m*/*z*. The molecular weight of **G2** was determined by using MALDI-TOF mass spectroscopy. It showed a series of major peaks at an m/z of around $MH^+$(3148.2 (100 %), and 3149.2) and $[M\text{-mpt}]^+$ (2989.1, 2990.1, and 2991.1).

### 2.2. Optical and Photoluminescence Spectra

Figure 1 shows the absorption spectra of ligands (in dichloromethane) and Ir complexes (in dichloromethane solution and in films). The photophysical properties of the ligands and the dendritic Ir complexes are listed in Table 1. The absorption spectra of the ligands are red-shifted because of the increase of conjugation with increasing generation number. The absorption spectra of the Ir complexes show intense bands in the ultraviolet region, which are assigned to spin-allowed ligand-centered transitions ($\pi$–$\pi^*$). Weak and broad absorption bands in the wavelength region longer than 400 nm are assigned to the $^1$MLCT and $^3$MLCT (metal-to-ligand charge transfer) due to spin-orbit coupling.[14b,20] In the absorption spectra of **G0**, both $^1(\pi$–$^*\pi)$ and MLCT bands in the solution and film show a similar shape. All dendritic Ir complexes (**G1-1**, **G1-2**, and **G2**) in solution show an absorption band similar to that of the free ligands. Compared with the absorption spectra in solution, except for complex **G0**, the ligand-centered $\pi$–$^*\pi$ transitions in the thin solid film are red-shifted by about 20 nm, obviously because of the increased intermolecular interaction between conjugated dendrons. The intensity of the MLCT transition is enhanced significantly in the solid film compared with that in the solution for all complexes except **G0**; this seems to indicate that the metal–ligand interaction increases in the solid films because of the existence of dendrons. It is not clear at this stage of the experiment why and how the incorporation of large dendrons could affect the MLCT oscillator strength. Further experiments are necessary in order to elucidate the origin. The photoluminescence (PL) spectra of the Ir complexes in dichloromethane solution with increasing generations from **G0** to **G1** to **G2** are red-shifted. More than 12 nm in the PL peak from **G0** to **G1-1** and 5 nm from **G1-1** to **G2** were observed (shown in Table 1). **G1-2** and **G2** show the same PL peak wavelength in solution although the UV spectra indicate that ligand **G2** has a larger conjugation (see Fig. 1, red-shifted absorption peak). The absolute PL efficiencies of the neat films were measured in an integrating sphere under the 325 nm line of a He–Cd laser. PL efficiencies in the film increased dramatically with dendrimer generation: 3.3 %, 21 %, 23 %, and 41 % for **G0**, **G1-1**, **G1-2**, and **G2**, respectively. It is obvious that T–T annihilation is significantly suppressed with an increase in the dendron size surrounding the cores.

### 2.3. Electrochemical Properties

Cyclic voltammetry (CV) was conducted at a scan rate of 10 $mV\,s^{-1}$ at room temperature (RT) under argon protection in deoxygenated 0.1–0.3 $mmol\,L^{-1}$ dichloromethane solution with 0.1 $mmol\,L^{-1}$ tetrabutylammonium hexafluorophosphate

ADVANCED FUNCTIONAL MATERIALS



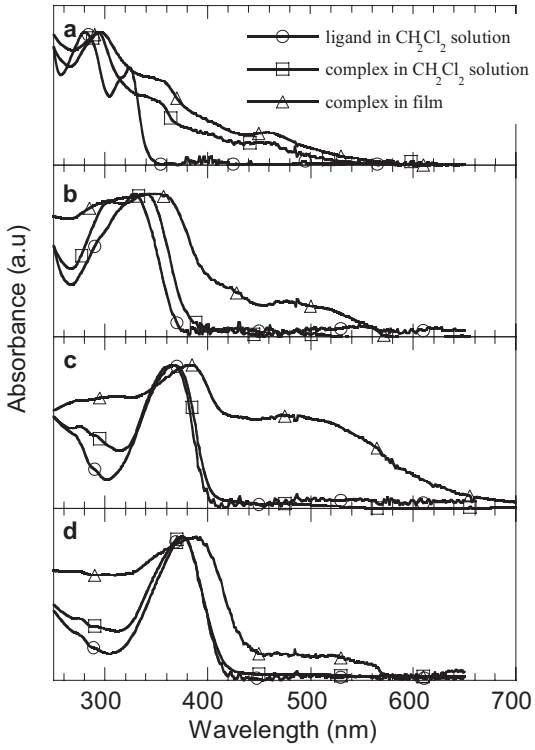


**Figure 1.** UV-vis absorption spectra of the ligands (in $CH_2Cl_2$) and dendrimers (in film and in $CH_2Cl_2$) **G0** (a), **G1-1** (b), **G1-2** (c), and **G2** (d)

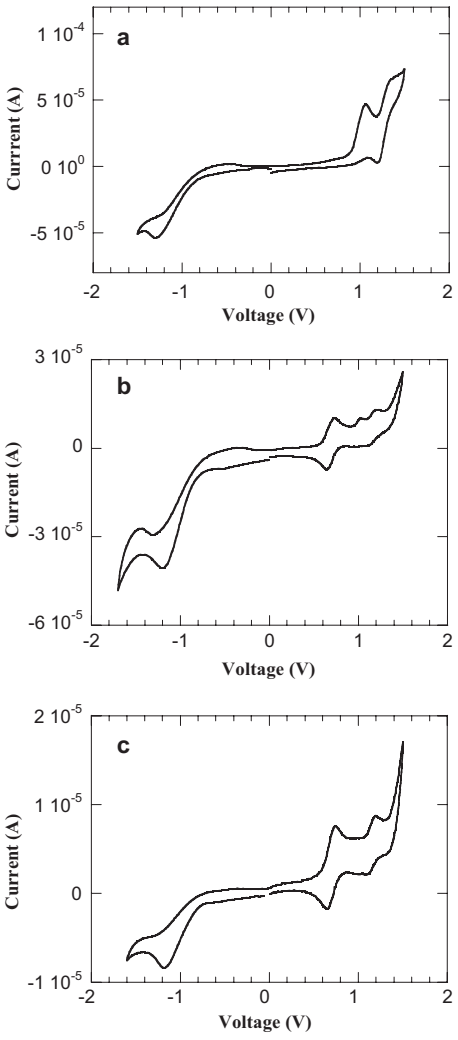


**Figure 2.** CV plots of **G0** (a), **G1-2** (b), and **G2** (c) (Scan rate: 10 $mVs^{-1}$, solvent: $CH_2Cl_2$).

($n$-$Bu_4NPF_6$) as the supporting electrolyte. Figure 2 shows the voltammogram of the dendritic Ir complexes. All Ir complexes showed reversible or quasi-reversible oxidation waves at ca. 0.5–1.5 V vs. a saturated calomel electrode (SCE). The measured oxidation potentials for **G0**, **G1-2**, and **G2** were 0.97, 0.56, and 0.54 V vs. SCE, respectively, which is mainly assigned to the oxidation of Ir metal cationic site (Ir(III)→Ir(IV)), together with a minor contribution from the cyclometalated ligand.[21,11a] Triarylamine-substituents attached to the cyclometalated ligand can affect the HOMO levels of dendrimers due to their interaction with the Ir d-orbital. The oxidation potential of the dendrimers was less positive than that of the corresponding core, indicating a lower ionization potential.[22] The oxidation of the triarylamine group in the dendritic Ir complexes also showed one or two reversible peaks in the higher-voltage oxidation region. The energy level and energy gap were calculated from the empirical formulae: $E_{HOMO} = -e(E_{ox} + 4.4)$, $E_{LUMO} = -e(E_{red} + 4.4)$, and $E_{gap} = E_{LUMO} - E_{HOMO}$ (where

**Table 1.** The optical and electrochemical properties of the complexes.

| Complexes | $E_{ox}$ [V] | $E_{red}$ [V] [a] | HOMO [ev] | LUMO [ev] | $E_{gap}$ [ev] | UV [nm] | PL [nm] | PL efficiency [%] [b] |
|---|---|---|---|---|---|---|---|---|
| **G0** | 0.97 | –1.44 | –5.37 | –2.96 | 2.41 | 233, 293, 353, 455 | 593 | 3.3 |
| **G1-1** | 0.68, 1.31 | –1.59 | –5.08 | –2.81 | 2.27 | 229, 305, 349 | 605 | 21 |
| **G1-2** | 0.56, 0.95, 1.10 | –1.45 | –4.96 | –2.95 | 2.01 | 230,366 | 610 | 23 |
| **G2** | 0.54, 1.14 | –1.56 | –4.94 | –2.84 | 2.10 | 230,375 | 610 | 41 |

[a] Quasi-reversible or irreversible; $E_{ox}$ and $E_{red}$ are the energies of the onset potential of oxidation and reduction, respectively They are calculated from the empirical formula, $E_{HOMO} = -(Eox + 4.40)$ (eV), $E_{LUMO} = -(E_{red} + 4.40)$ (eV) (see main text). The UV and photoluminescence (PL) data were obtained in $CH_2Cl_2$ solution. [b] Measured in the integrating sphere under a 325 nm line of a HeCd laser.

$E_{HOMO}$ is the energy level of the highest occupied molecular orbital (HOMO), $E_{LUMO}$ is the energy level of the lowest unoccupied molecular orbital (LUMO), $E_{gap}$ is the energy gap, $E_{ox}$ is the oxidation potential, and $E_{red}$ the reduction potential.[23] Although the measured redox potentials from solution to thin films generally increase by tenths of electronvolts (ca. 0.2 eV), solution CV measurements are fairly applicable to the discussion of energy levels in thin film OLEDs.[24] The data collected in Table 1 show that the oxidation potential of Ir(III) decreases with increasing $\pi$-conjugation of the dendrons, which is consistent with the data from the UV-vis and PL spectra.

### 2.4. Electroluminescent Properties

The devices of the dendritic Ir complexes **G1-2** and **G2** were fabricated by spin-coating from chloroform solution with the following device structures: 1) ITO/dendrimer:CBP (2:8)/TPBI/LiF/Al; 2) ITO/PEDOT/dendrimer:CBP (2:8)/TPBI/LiF/Al; 3) ITO/PEDOT/PVK/dendrimer:CBP (2:8)/TPBI/LiF/Al (PVK = poly(vinylcarbazole), PEDOT = poly(3,4-ethylenedioxythiophene), and ITO = indium tin oxide), where CBP was used as the host and TPBI was used as the electron-transporting/hole-blocking material. Figure 3a shows the PL spectra of the host (CBP), **G1-2:**CBP (2:8), and **G2**:CBP (2:8) films under 325 nm excitation of a HeCd laser. The PL profiles of **G1-2/**CBP and **G2/**CBP blends contain only one peak at about 615 nm with a vibronic shoulder at 653 nm resulting from triplet emission. Figure 3b,c shows the EL spectra of different devices for G1-2, G2. The fact that no emission from the host CBP appeared in the Ir-complex doped blend film indicated complete energy transfer from CBP to the Ir complex. Figure 4 shows the EQE ($Q$)–luminance ($L$)–current density ($J$) characteristics for **G1-2/**CBP and **G2/**CBP blend in different device structures. The results revealed that the devices (type 1) without PEDOT and PVK layers performed better. On the other hand, the devices with a PVK layer showed a much higher turn-on voltage. Maximum EQEs of 12.8% and 11.8% photons/electron (ph/el) and maximum luminous efficiencies 9.2 cd $A^{-1}$ and 8.5 cd $A^{-1}$ for **G1-2** and **G2**, respectively were obtained at 0.1 mA $cm^{-2}$ with a brightness of 13 cd $m^{-2}$. If no electron-transporting/hole-blocking material (TPBI) was deposited at the top of the dendrimer-containing film, the devices exhibited much poorer performance.

The electroluminescence (EL) performance of devices from the dendrimers of different generations (**G1-2** and **G2**) with different anode buffer layers is compared at the same current density of 30 mA $cm^{-2}$ in Table 2. The comparable device performance obtained for these devices with or without anode buffers (a hole-transporting layer (HTL) layer) of different work function: (ITO, 4.8–4.9 eV; PEDOT, 5.0–5.2 eV; and PVK, 5.67–5.8 eV) indicates that hole-injection is not a limiting factor in these devices. This is consistent with the low HOMO levels of such dendrimers (4.9 eV, Table 1). The best device performance, with a brightness of nearly 3900 cd $m^{-2}$, was obtained for **G1-2** and **G2** in device 1 with ITO as an anode without a HTL layer. We note that **G1-2** showed comparable device

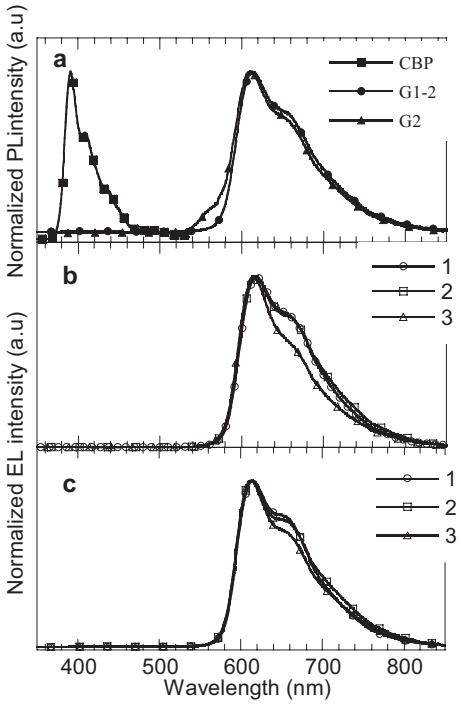


**Figure 3.** PL spectra of the host (CBP), **G1-2** (20 wt%) + CBP, and G2 + CBP (20 wt%) (a), and EL spectra of different devices for **G1-2** (b) and **G2** (c). The device structures were: 1) ITO/(dendrimer:CBP (2:8))/TPBI/LiF/Al; 2) ITO/PEDOT/(dendrimer:CBP (2:8))/TPBI/LiF/Al; and 3) ITO/PEDOT/PVK/(dendrimer:CBP (2:8))/TPBI/LiF/Al.

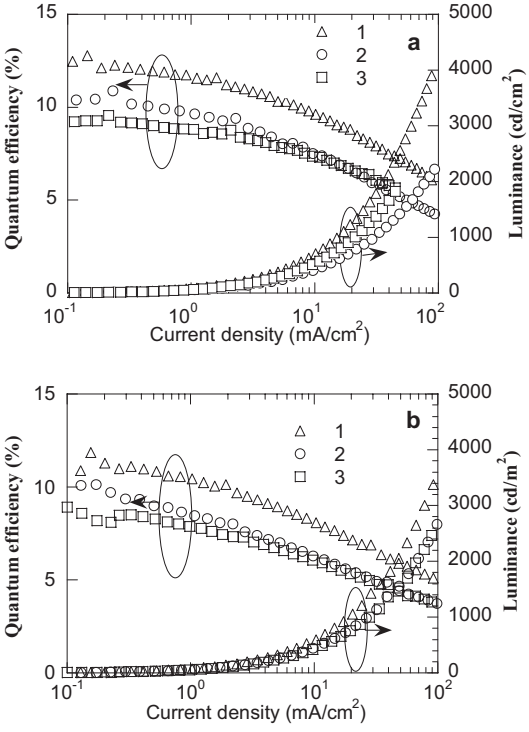


**Figure 4.** The EQE ($Q$)–luminance ($L$)–current density ($J$) with different structures of a) **G1-2** and b) **G2**. The device structures are 1) ITO/(dendrimer:CBP (2:8))/TPBI/LiF/Al; 2) ITO/PEDOT/(dendrimer:CBP (2:8))/TPBI/LiF/Al; and 3) ITO/PEDOT/PVK/(dendrimer:CBP (2:8))/TPBI/LiF/Al.

ADVANCED FUNCTIONAL MATERIALS



**Table 2.** Device performances of the Ir complexes doped in the CBP host. The devices are: 1) ITO/(dendrimer:CBP (2:8))/TPBI/LiF/Al; 2) ITO/PEDOT/(dendrimer:CBP (2:8))/TPBI/LiF/Al; and 3) ITO/PEDOT/PVK/(dendrimer:CBP (2:8))/TPBI/LiF/Al.

| Materials | Device No. | Maximum QE | | | | J=30 mA/cm$^2$ | | | |
|---|---|---|---|---|---|---|---|---|---|
| | | Volt [V] | L. [cd m$^{-2}$] | QE [%] | L [cd A$^{-1}$] | Voltage [V] | L. [cd m$^{-2}$] | QE [%] | L [cd A$^{-1}$] |
| | 1 | 15.5 | 13 | 12.8 | 9.2 | 31 | 1789 | 7.9 | 5.7 |
| **G1-2** | 2 | 11.2 | 14 | 10.9 | 6.1 | 22.3 | 1087 | 5.8 | 3.3 |
| | 3 | 25.0 | 15 | 9.6 | 6.9 | 40.5 | 1374 | 6.1 | 4.4 |
| | 1 | 17.5 | 13 | 11.8 | 8.5 | 30.5 | 1427 | 6.9 | 5.0 |
| **G2** | 2 | 14.5 | 1.3 | 11.3 | 8.1 | 30 | 1136 | 4.9 | 3.5 |
| | 3 | 18.0 | 2 | 9.3 | 6.7 | 34.5 | 1150 | 4.8 | 3.4 |

performance to **G2**, although PL efficiencies of these films were quite different, which is different from the result found by previous reports,[5b,9] where a significant difference in EL performance was observed for the dendrimers of different generations. It indicates that carrier balance dominates device performance in these devices created from dendrimers doped into a small molecule host. Although devices from a 20 wt % blend of **G0** in CBP were also fabricated, they were observed to have poor performance (EQE < 0.5 %) due to poor film quality. This further showed that the modified dendrons attached to the core optimized the EL performance for devices processed by using spin-coating technology.

For comparison, we also utilized a blue-emitting polymer PFO (in the presence of 30 % PBD)[25] as the host for **G0**, **G1-1**, and **G1-2**. The device configuration was ITO/PEDOT/PVK/blends/Ba/Al. The doping concentration of Ir complexes in the host was 1 %, 2 %, 4 %, 8 % and 16 %. Figure 5 shows the PL spectra of **G1-2** blend films and EL spectra of the devices with different doped concentrations. A complete quenching of the host PL emission occurred at 8 % doping concentration, whereas the host EL peak was completely quenched at a doping concentration as low as 1 %, much lower than what was observed in the PL spectra. The fact that complete quenching of the host EL emission occurred at a much lower doping concentration has been attributed by some references[26] to the charge-trapping mechanism (rather than to Förster energy transfer) followed by recombination on the chromophore (Ir complex). The best device performance of **G0**, **G1-1**, and **G1-2** is listed in Table 3. The best device performance was observed at 8 % (**G1-1**) or 16 % (**G1-2**) doping concentration. For **G1-1**, the maximum EQE, luminance efficiency and luminance are 12.3% ph/el, 8.4 cd A$^{-1}$, 2369 cd m$^{-2}$ at 6.5 mA/cm$^{-2}$, and for **G2**, those parameters are 13.9%, 9.5 cd A$^{-1}$, 601 cd m$^{-2}$ at 6.4 mA cm$^{-2}$, respectively. At 100 mA cm$^{-2}$, the efficiency of **G1-1** remained as high as 10.4 % and 7.7 cd A$^{-1}$ at a luminance of 7577 cd m$^{-2}$. The maximum luminance of the device for **G1-1** (8 % doping) exceeds 12 537 cd m$^{-2}$ at 253 mA cm$^{-2}$ with a quantum efficiency (QE) = 6.7 %. The device maintained high efficiency at a high current density. For example, device efficiency from **G1-2** (16 % doping) remained at QE = 5.4 % with a luminance of 10 699 cd m$^{-2}$ at 288 mA cm$^{-2}$. As the molecular weights of the dendrimers of different concentrations were quite different, in order to compare device performance of different generations, it is more rational to use devices from blend films with similar guest/host molar ratio (per host polymer unit). In Figure 6 we compare EQE vs. current density for two sets of devices from **G0**, **G1-1**, and **G1-2** at molar concentration of around 0.5 % (molar). It can be seen from Figure 6 that device efficiencies greatly increase with the increase of dendrimer generation for devices with approximately the same doping concentration (molar). This indicates that with increasing dendrimer generations, the possibility of aggregations of Ir cores and T–T annihilation is greatly reduced. This is also consistent with the increased PL quantum efficiency with dendrimer generations (Table 1). Compared with the device performance of the dendrimers doped into a small molecule host (CBP; Table 2), we note that the efficiency of the devices with a polymer host (PFO; Table 3) is generally higher. The efficiency decay speed with increasing current density has a gentler slope for devices with a polymer host. This indicates that, because of the attached bulky dendrons, dendrimers have a good intermolecular interaction with the polymer host in solution and tend to have less self-aggregation upon film formation. As a result, the concentration quenching at high dopant concen-

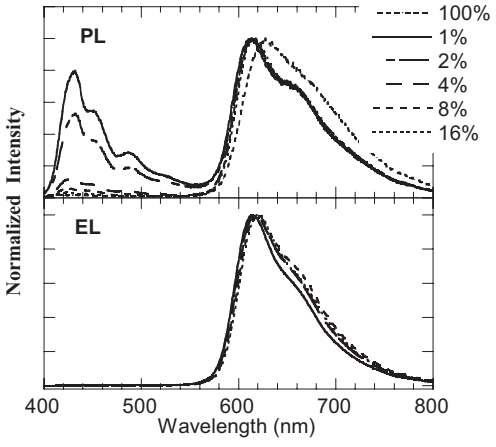


**Figure 5.** The PL and EL spectra of **G1-2** doped into PFO (30 % PBD).

**Table 3** Device performances of Ir dendrimer doped into a polymer host (PFO). The device structure was ITO/PEDOT (40 nm)/PVK (40 nm)/blends (70–80 nm)/Ba (5 nm)/Al (200 nm)

| Material | Doping [%] | | Maximum QE | | | | | J = 100 mA cm$^{-2}$ | | | |
|---|---|---|---|---|---|---|---|---|---|---|---|
| | Ir-complex/PFO weight ratio | Iridium/PFO Molar ratio | V [V] | J [mA cm$^{-2}$] | L [cd m$^{-2}$] | LE [cd A$^{-1}$] | QE [%] | V [V] | L [cd m$^{-2}$] | LE [cd A$^{-1}$] | QE [%] |
| **G0** | 2 | 0.51 | 11.4 | 15.9 | 831 | 5.2 | 7.0 | 13.4 | 4342 | 4.2 | 5.6 |
| **G0** | 4 | 1.01 | 13.8 | 8.2 | 480 | 5.8 | 7.9 | 16.8 | 5511 | 5.3 | 7.2 |
| **G0** | 8 | 2.02 | 12.8 | 14.0 | 853 | 6.1 | 8.2 | 15.0 | 5395 | 5.1 | 6.8 |
| **G1-1** | 2 | 0.31 | 18.9 | 57.4 | 2953 | 7.0 | 5.2 | 19.3 | 4273 | 6.4 | 4.7 |
| **G1-1** | 4 | 0.62 | 19.4 | 65.7 | 3976 | 8.2 | 6.1 | 20.2 | 6384 | 5.7 | 7.8 |
| **G1-1** | 8 | 1.23 | 18.5 | 29.3 | 2369 | 8.1 | 10.9 | 20.6 | 7577 | 7.7 | 10.4 |
| **G1-2** | 4 | 0.45 | 13.6 | 6.5 | 562 | 8.6 | 12.6 | 17.9 | 6340 | 6.4 | 9.3 |
| **G1-2** | 8 | 0.90 | 16.4 | 6.5 | 544 | 8.4 | 12.3 | 21.6 | 5847 | 5.8 | 8.5 |
| **G1-2** | 16 | 1.80 | 13.9 | 6.4 | 601 | 9.5 | 13.9 | 19.3 | 7179 | 6.5 | 9.5 |

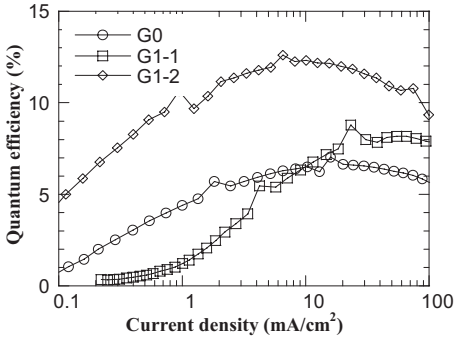


**Figure 6.** The quantum-efficiency–current-density curves of **G0** (Ir%: 0.51), **G1-1** (Ir%: 0.62), **G1-2** (Ir%: 0.45); the device structure was ITO/PEDOT (40 nm)/PVK (40 nm)/blends (70–80 nm)/Ba (5 nm)/Al (200 nm).

tration and T–T annihilation at high current density are significantly suppressed.[26]

## 3. Conclusions

We have reported a detailed study of the synthesis and photophysical and phosphorescent properties of new iridium dendrimers with charge-transporting dendrons. The first- and second-generation dendrimers, which were doped in CBP at a ratio of 20 wt %, showed high efficiencies in two-layer OLEDs fabricated with spin-coating. In addition, for comparison, we also fabricated the dendrimer doped in the polymer host PFO with **G0**, **G1-1**, and **G1-2**. The results indicated that charge-transport dendrons and surface-group modification were very important for not only the solubility but also the EL performance. **G1-2** and **G2** showed similar very good performance, with maximum external quantum efficiencies of 12.8% and 11.8% (ph/el) and luminous efficiency of 9.2 cd A$^{-1}$ and 8.5 cd A$^{-1}$ with red emission peaked at 610 nm for **G1-2** and **G-2**, respectively. To the best of our knowledge, this is the highest record of a red phosphorescent device fabricated by using solution processing.

## 4. Experimental

### 4.1. Measurement and Characterization

The $^1$H NMR spectra were collected on a Bruker DRX 400 and a Bruker DRX 300 spectrometer in deuterated chloroform. GC-MS spectra were recorded by using a Trace 2000 Series (CE Instruments company); ESI-MS spectra were recorded on a LCQ DECA XP liquid-chromatography mass spectrometry (Thremo Group); MALDI-TOF mass was recorded on a Voyager DEPRO MALDI-TOF spectrometer (Applied Biosystems). Elemental analysis was carried out with a Vario EL elementary analyzer. UV-vis absorption spectra were recorded on a HP 8453 UV-vis spectrophotometer. CV were carried out on a CHI660A electrochemical workstation.

### 4.2. Device Fabrication and Characterization

The dendrimer + CBP electrophosphorescent configurations were 1) ITO/dendrimer:CBP (2:8)/TPBI/LiF/Al; 2 ITO/PEDOT/dendrimer:CBP (2:8)/TPBI/LiF/Al; 3) ITO/PEDOT/PVK/dendrimer:CBP (2:8)/TPBI/LiF/Al. The fabrication of these devices was as follows: The ITO–glass substrate was precleaned by using oxygen plasma. A 60 nm thick layer of PEDOT (Baytron P 4083) was spin-cast onto a precleaned ITO–glass substrate. Then, a 40 nm thick layer of PVK was spin-cast onto the top of PEDOT. A mixture of the Ir complex with CBP was spin-cast from the solution in chloroform with a 70 nm thick layer. The electron-transporting layer TPBI was evaporated until 50 nm thick. The cathode comprised lithium fluoride (LiF) (1 nm) and aluminum layers (150 nm).

The polymer device configuration was ITO/PEDOT (40 nm)/PVK (40 nm)/blends (70–80 nm)/Ba (5 nm)/Al (200 nm). The fabrication of electrophosphorescent devices followed the method reported previously [19].

Profilometer (Tencor Alfa-Step 500) was used to determine the thickness of the films. Layer thickness during thermal deposition was monitored upon deposition by using a crystal thickness monitor (Sycon). Device fabrication was carried out in a controlled dry-box (Vacuum Atmosphere Co.) in $N_2$ circulation. Current density (J)–voltage (V)–luminance (L) data were collected with a Keithley 236 source measurement unit and a calibrated silicon photodiode. Absolute photo-

luminescent efficiencies were measured in the integrating sphere (IS-080, Labsphere) under the 325 nm line of a HeCd laser. External electroluminescent QEs were obtained by measuring the total light output in all directions in an integrating sphere (IS-080, Labsphere). The luminance (cd $m^{-2}$) was measured by using a Si photodiode, and calibrated by using a PR–705 Spectra Scan Spectrophotometer (Photo Research). PL and EL spectra were recorded by using a charge-coupled device (CCD) spectrophotometer (Instaspec 4, Oriel).

### 4.3. Reagents

All reagents and solvents were obtained from Aldrich, Acros, and TCI Chemical Co. and used as received. The solvents were treated as required prior to use.

### 4.4. Synthesis

The synthetic routes of the ligands and Ir complexes are shown in Schemes 1 and 2.

#### *4.4.1. 3-Bromo-N-phenethyl benzamide (**1**)*

3–bromobenzoyl chloride (12.0 g, 54.7 mmol) was dropped into a mixture of phenethylamine (9.3 g, 76.7 mmol) and triethylamine (10.0 g, 0.1 mol) in 80 mL of dichloromethane. The mixture was stirred at RT for 4 h. After being washed successively with water, 5 % hydrochloric acid, and water, the organic layer was dried with anhydrous magnesium sulfate. The obtained product was purified by recrystallization from ethyl acetate to give a white powder (12.5 g, 75.3 %). GC-MS, m/z, 304, M+. $^1$H NMR $\delta$ (300 MHz, $CDCl_3$): 7.83–7.82 (1H, t), 7.59–7.56 (2H, m), 7.42–7.30 (2H, t), 7.27–7.23 (2H, m), 7.23–7.20 (2H, t), 6.19 (1H, s) 3.71–3.66 (2H, t), 2.93–2.89 (2H, t).

#### *4.4.2. 1-(3-Bromophenyl)-3,4-dihydroisoquinoline (**2**)*

Phosphorus pentoxide (28.6 g, 0.1 mol) and phosphorus oxychloride (80 mL) were added to the solution of **1** (6.0 g, 0.02 mol) dissolved in 40 mL of xylene with stirring. The mixture was heated to reflux and continued for 3 h. After being cooled to RT, the solvent was decanted and the residual solid was carefully triturated to neutrality with 10 % sodium hydroxide solution. The resultant aqueous mixture was extracted with dichloromethane. Further purification by silica gel column chromatography using ethyl acetate/dichloromethane (3:1) as the eluent gave **2** as a pale yellow oil (4.56 g, 80.7 %). GC-MS: m/z 286, M+. $^1$H NMR $\delta$ (300 MHz, $CDCl_3$): 7.76–7.75 (1H, t), 7.59–7.55 (1H, dd), 7.54–7.51 (1H, m), 7.42–7.38 (1H, m), 7.31–7.28 (2H, d), 7.27–7.21 (2H, m), 3.87–3.83 (2H, t), 2.82–2.79 (2H, t).

#### *4.4.3. 4-Bromo-N,N-diphenylaniline (**3**)*

Diphenylamine (19.3 g, 114 mmol), 4-bromoiodobenzene (32.2 g, 114 mmol), 1.12 g 1,10-phenanthroline, 0.62 g copper(I), and 49.6 g potassium hydroxide flakes were added to a mixture of xylene (100 mL) and toluene (50 mL). The apparatus was purged with Ar and then heated rapidly to rigorous reflux. After refluxing for 48 h, the reaction mixture was cooled to 75 °C and added to a mixture of toluene and water (50:100 mL). The organic phase was separated, washed further with a portion of water (100 mL), and dried with anhydrous magnesium sulfate. The solvent was removed under reduced pressure to give a black solid. It was purified by using silica gel column chromatography by using petroleum ether as the eluent to obtain a colorless solid (21.1 g, 57.2 %) [27]. GC-MS: m/z, 324, $M^+$. $^1$H NMR (300 MHz, $CDCl_3$), $\delta$(ppm): 7.33–7.30 (m, 2H), 7.29–7.26 (t, 4H), 7.10–7.07 (d, 4H), 7.04–7.02 (d, 2H), 6.96–6.92 (m, 2H).

#### *4.4.4. 4-(4,4,5,5-tetramethyl-1,3,2-dioxaborolan-2-yl)-N,N-diphenylaniline (**4**)*

**3** (9.72 g, 30 mmol) was dissolved in tetrahydrofuran (THF; 150 mL) and cooled to –78 °C and 12.5 mL of 2.87 M *n*-BuLi solution in hexane (36 mmol, 1.2 eq.) was slowly dropped into it. The resulting solution was allowed to warm to 0 °C until a clear-yellow solution was formed. The solution was cooled back to –78 °C. 2-Isopropoxy-4,4,5,5-tetramethyl-1,3,2-dioxaborolane (16.75 g, 90 mmol) was added and a white suspension was formed after 1 h. The mixture was warmed to RT and stirred for 24 h. The mixture was poured into water and extracted with ethyl ether. The organic layer was dried by magnesium sulfate. Silica gel column chromatography with petroleum ether as the eluent isolated a white powder (7.77 g, 69.8 %). GC-MS: m/z, 371, $M^+$. $^1$H NMR (300 MHz, $CDCl_3$), $\delta$ (ppm): 7.70–7.67 (m, 2H), 7.30–7.27 (m, 4H), 7.14–7.11 (m, 4H), 7.09–7.03 (m, 4H), 1.35 (s, 12H).

#### *4.4.5. N,N-diphenyl-3′-(3′,4′-dihydoisoquinolin)-4-biphenylaniline (**5**)*

A solution of 3.40 g (11.9 mmol) of **2**, 4.86 g (1.31 mmol) of **4**, 6.6 ml of 2 M sodium carbonate, 60 mL of toluene, and 30 mL of ethanol were degassed with Ar for 20 min, and then 0.303 g of $Pd(PPh_3)_4$ were added. The solution was refluxed for 24 h under Ar. After being cooled to RT, 10 mL of water was added. The aqueous layer was extracted with dichloromethane (15 mL × 3) and dried with anhydrous magnesium sulfate. The product was purified by silica-gel column chromatography using ethyl acetate/dichloromethane (1/9) as the eluent and dried in vacuum to give a yellow power (4.46 g, 83.2 %). GC-MS: m/z, 449.2, [M–1]+. $^1$H NMR (300 MHz, $CDCl_3$), $\delta$ (ppm): 7.83 (s, 1H), 7.69 (d, 1H), 7.50–7.58 (m, 4H), 7.44–7.40 (m, 1H), 7.27–7.37 (m, 7H), 7.14–7.16 (d, 6H), 7.03–7.07 (m, 2H), 3.86–3.93 (t, 2H), 2.81–2.88 (t, 2H).

#### *4.4.6. N,N-Diphenyl-3′-isoquinolinyl-4-biphenylaniline (**6**, **L-G1-1**)*

2.86 g (6.4 mmol) **5** was dissolved in 20 mL of mesitylene and 0.180 g 10 % Pd/C was added. It was refluxed for 3 h at 190 °C under Ar. After being cooled to RT, the solution was filtered and the black power was washed with dichloromethane several times. The product was purified by recrystallization from the petroleum ether and dried to give a pale powder (1.69 g, 59.4 %). GC-MS: m/z, 447.2, $[M-1]^+$. $^1$H NMR (400 MHz, $CDCl_3$) $\delta$ (ppm): 8.67 (d, 1H), 8.21 (d, 1H), 7.95 (d, 2H), 7.75 (t, 3 H), 7.73–7.56 (m, 6H), 7.30–7.26 (m, 2H), 7.17–7.14 (m, 6H), 7.06–7.04 (t, 3H).

#### *4.4.7. N,N-di(p-bromophenyl)-3′-isoquinolinyl-4-biphenylaniline (**7**)*

1.05 g (2.34 mmol) of **6** were dissolved in 10 mL of chloroform, and 0.876 g (4.68 mmol) of *N*-bromosuccinimide in chloroform was added dropwise to the solution. It was stirred at RT for 3 h. The product was purified by silica-gel column chromatography using ethyl acetate/dichloromethane (1/9) as the eluent to give a yellow power (1.12 g, 78.9 %). ESI-MS: m/z, 607.2, [M+1]+. 1H NMR (300 MHz, CDCl3), $\delta$ (ppm): 8.64–8.63 (d, 1H), 8.17–8.16 (d, 1H), 7.92–7.90 (d, 2H), 7.72–7.65 (m, 4H), 7.61–7.54 (m, 4H), 7.37–7.33 (m, 4H), 7.12–7.10 (t, 2H), 6.99–6.97 (t, 4H).

#### *4.4.8. N,N-Di(9,9-dimethylfluorenyl)-4-(4,4,5,5-tetramethyl-1,3,2-dioxaborolan-2′-yl)aniline (**9**)*

The solution of 4.43 g (7.97 mmol) **8** in 110 mL of THF was cooled to –78 °C, and 3.32 mL of 2.87 M *n*-BuLi in hexane (9.57 mmol, 1.2 eq.)

was dropped in slowly. The solution was warmed to RT, then cooled to –78 °C again, 4.45 g (23.9 mmol) of 2-isopropoxy-4,4,5,5-tetramethyl-1,3,2-dioxaborolane was injected. The mixture was warmed to the RT slowly and stirred for 24 h. The mixture was poured into water and extracted with ethyl ether. The organic layer was washed with brine and dried over anhydrous magnesium sulfate. It was purified further by silica-gel column chromatography using ethyl acetate/hexane (1/9) as the eluent to give a pale powder (2.8 g, 63.2 %). $^1$H NMR (300 MHz, $CDCl_3$) $\delta$ (ppm): 7.74–7.73 (d, 2H), 7.69–7.67 (d, 2H), 7.61–7.59 (d, 2H), 7.42–7.40 (d, 2H), 7.36–7.32 (m, 2H), 7.32–7.31 (d, 2H), 7.28–7.26 (m, 2H), 7.13–7.12 (d, 2H), 7.12–7.10 (d, 2H), 1.43 (s, 12H), 1.37 (s, 12H).

#### *4.4.9. N,N-di(9,9-dimethylfluorenyl)-3′-(3′,4′-dihydoisoquinolin)-4-biphenylaniline (***10***)*

1.525 g (5.3 mmol) of **2**, 2.9 g (4.8 mmol) of **9**, and 2.5 mL of 2 M sodium carbonate were dissolved in 30 mL of *N,N*-dimethylformamide. After being degassed for 20 min, 0.110 g of $Pd(PPh_3)_4$ was added. The mixture was refluxed for 24 h under Ar. Then 10 mL of water was added after the solution cooled down. The aqueous layer was extracted with dichloromethane (15 mL × 3) and dried with anhydrous magnesium sulfate. The product was purified by silica-gel column chromatography using dichloromethane/petroleum ether (1/9) as the eluent and dried in vacuum to give a yellow power (2.12 g, 65.2 %). ESI-MS: m/z, 683.4, $[M+1]^+$. $^1$H NMR (300 MHz $CDCl_3$), $\delta$ (ppm): 7.88 (s, 1H), 7.73–7.72 (d, 1H), 7.68–7.67 (d, 2H), 7.63–7.62 (d, 2H), 7.58–7.53 (m, 4H), 7.46–7.35 (m, 5H), 7.34–7.25 (m, 9H), 7.15–7.12 (m, 2H), 3.89–3.87 (t, 2H), 2.85–2.82 (t, 2H), 1.44 (s, 12H).

#### *4.4.10. N,N-di(9,9-dimethylfluorenyl-3′-isoquinolin-4-biphenylaniline (***11***,* **L-G1-2***)*

1.76 g (2.6 mmol) of **10** was dissolved in 20 mL of mesitylene and 0.055 g of 10 % Pd/C was added. The mixture was refluxed for 3 h at 190 °C under Ar. The product was purified by column chromatography over silica-gel using acetyl acetate/dichloromethane (1/9) as the eluent and dried in vacuum to give a yellow power (1.45 g, 83.0 %). ESI-MS: m/z, 681.5, [M+1]+. $^1$H NMR ($CDCl_3$, 300 MHz), $\delta$ (ppm): 8.67–8.65 (d, 1H), 8.19–8.16 (d, 1 H), 7.96 (s, 1 H), 7.94–7.92 (d, 1H), 7.76–7.75 (m, 12H), 7.42–7.41 (d, 2 H), 7.35–7.31 (m, 2H), 7.30–7.25 (m, 6H), 7.16–7.13 (m, 2H), 1.44 (s, 12H).

#### *4.4.11. N,N-di(4′-di(2′-(9′,9′-dimethylfluorenyl)amine)biphenyl-3′-isoquinolinyl-4-biphenylaniline (***12***,* **L-G2***)*

0.909 g (1.5 mmol) of **7**, 1.81 g (3 mmol) of **9**, and 3 mL of 2 M sodium carbonate solution were added to the solvent of 30 mL of toluene and 15 mL of ethanol. The mixture was degassed for 20 min. To the solution was added 0.069 g $Pd(PPh_3)_4$. The mixture was refluxed for 24 h under Ar. Then 10 mL of water was added after the solution cooled down. The aqueous layer was extracted with dichloromethane (15 mL × 3) and dried with anhydrous magnesium sulfate. The product was purified by using silica-gel column chromatography using dichloromethane/petroleum ether (1/9) as the eluent and dried in vacuum to give a yellow powder (1.43 g, 68.0 %). ESI-MS: m/z, 1398.6 (100 %), M+, 1 H NMR ($CDCl_3$, 300 MHz), $\delta$ (ppm): 8.66 (d, 1H), 8.21 (d, 1H), 7.95–7.92 (m, 2H), 7.76–7.72 (m, 3H), 7.64–7.60 (m, 13H), 7.56–7.51 (m, 8H), 7.40 (d, 4H), 7.34–7.30 (m, 5H), 7.28–7.25 (m, 17H), 7.14 (d, 4H), 1.43 (s, 24H).

#### *4.4.12. 5-methyl-3-(pyridin-2-yl)-1 H-1,2,4-triazole (***13***)*

10 mL of 80 % hydrous hydrazine was added to a flask containing 6.2 g of 2-cyanopyridine. The solution was heated to 40 °C for 3 h and the solvent was removed by decanting. 10 mL of acetic acid was dropped into the residue. The solution was stirred at RT for 1 h, then heated to reflux for 3 h. After being cooled to RT, the solvent was removed to obtain a white solid. Further purification was achieved by recrystallization from water. $^1$H NMR ($CDCl_3$, 400 MHz): $\delta$ (ppm): 8.76–8.75 (d, 1H), 8.25–8.24 (d, 1H), 8.13 (s, 1H), 7.90–7.88 (t, 1H), 7.42–7.40 (t, 1H), 2.43(s, 3H), GC-MS: m/z, 160, M+.

#### *4.4.13. Iridium Complexes*

Cyclometalated Ir(III) chloro-bridged dimers of general formula $(C^N)_2Ir(\mu\text{-}Cl)_2Ir(C^N)_2$ (where C^N represents a cyclometalating ligand) were synthesized by the method reported by Tamayo et al. [21]. $IrCl_3.3H_2O$ was heated to 110 °C with a 2–2.5 equivalent of cyclometalating ligand in a 3:1 mixture of 2-ethoxyethanol under argon for 24 h. The crude yield exceeded 85 %.

#### *4.4.14.* **G0** *Bis(1-Phenylisoquinoline-C2,N′) iridium(III((5-methyl-3-(pyridin-2′-yl)-1,2,4-triazole)*

A solution of 0.80 g (5.0 mmol) of **13** and 0.27 g (5.0 mmol) of sodium methoxide in 50 mL of anhydrous ethanol was heated to 50 °C for 1 h. 0.502 g (0.4 mmol) of chloro-bridged dimer in 10 mL of dichloromethane was dropped into the solution. The reacting mixture was refluxed for 3 h and cooled down to RT. 50 mL of water and 30 mL of dichloromethane were added and the organic layer was washed with water, and then dried with anhydrous magnesium sulfate. Further purification by using silica gel column chromatography using acetone/dichloromethane (1:1) as the eluent gave a red power 0.427 g, 71.5 %. ESI-MS: m/z, 761.3, [m+1]+. $^1$H NMR(400 MHz, $CDCl_3$), $\delta$ (ppm): 8.95—8.94 (m,1H), 8.90–8.88 (m, 1H), 8.25–8.15 (m, 3H), 7.83–7.76 (m, 2H), 7.76–7.74 (m, 2H), 7.69–7.66 (m, 4H), 7.48–7.46 (d, 1H), 7.43–7.41(d, 1H), 7.26–7.25 (d, 1H), 7.16–7.15 (d, 1H), 7.02–6.97 (m, 3H), 6.84–6.78 (m, 2H), 6.39–6.35 (m, 2H), 2.43 (s, 3H). Calcd for $C_{38}H_{27}IrN_6$: C, 60.1; H, 3.6; N, 11.1. Found: C, 59.9; H, 3.8; N, 10.6.

#### *4.4.15.* **G1-1**

Synthesis details of dendrimer **G1-1** were similar to those described for **G0**. The crude product was separated by using silica column chromatography using acetone/dichloromethane (1:1) as the eluent to give a red power (isolated yield, 52.6 %). EI-MS: m/z, 1247.5, (M+1)+, $^1$H NMR $\delta$ ($CDCl_3$, 300 MHz): $\delta$ (ppm): 9.07–9.05 (m, 1H), 9.02–9.00 (m, 1H), 8.46 (s, 2H), 8.28 (s, 1H), 7.9–17.74 (m, 9H), 7.60–7.59 (d, 1H), 7.51–7.48 (m, 3H), 7.45–7.43 (d, 2H), 7.35–7.33 (d, 1H), 7.29–7.23 (m, 7H), 7.15–7.09 (m, 14H), 7.06–6.99 (m, 6H), 6.51–6.49 (t, 2H), 2.49 (s, 3H). Calcd for $C_{74}H_{53}IrN_8$: C, 71.3; H, 4.3; N, 9.0. Found: C, 70.9; H, 4.5; N, 8.8.

#### *4.4.16.* **G1-2**

Synthesis details of dendrimer **G1-2** were similar to those described for **G0**. The crude product was separated by using silica column chromatography using acetone/dichloromethane (2:1) as the eluent to give a red power, (isolated yield 38 %). ESI-MS: m/z 1711.3, [M+1]+. $^1$H NMR (300 MHz, $CDCl_3$), $\delta$ (ppm): 9.11–9.03 (m, 2H), 8.51 (s, 2H), 7.93–7.90 (m, 4H), 7.87–7.83 (m, 4H), 7.77–7.74 (m, 4 H), 7.67–7.60 (m, 10H), 7.57–7.48 (m, 6H), 7.42–7.24 (m, 16H), 7.21–7.18 (m, 2H), 7.18-7.09 (m, 6H), 6.54–6.47 (m, 2H), 2.52 (s, 3H), 1.43 (s, 24H). Calcd for $C_{110}H_{85}IrN_8$. C, 77.2; H, 5.0; N, 6.6. Found: C, 76.7; H, 5.0; N, 6.5.

#### *4.4.17.* **G2**

Synthesis details of dendrimer **G2** were similar to those described for **G0**. The crude product was separated by using silica column chromatography using acetone/dichloromethane (5:1) as the eluent to give a red power (isolated yield 21 %). MALDI-TOF: MH+: 3148.2 (100 %), 3149.2, [M-mpt]+ (2989.1, 2990.1, 2991.1), $^1$H NMR

($CDCl_3$, 400 MHz), $\delta$ (ppm): 9.11–9.02 (m, 2H), 8.49 (s, 2H), 7.94–7.84 (m, 4H), 7.81–7.70 (m, 6H), 7.68–7.61 (m, 16H), 7.57–7.46 (m, 20H), 7.42 (d, 8H), 7.36 (d, 6H), 7.31–7.15 (m, 40H), 7.13–7.09 (m, 8H), 7.06–7.04 (m, 4H), 6.54–6.47 (m, 2H), 2.52 (s, 3H), 1.41 (s, 48H). Calcd for $C_{218}H_{169}IrN_{12}$: C, 83.2; H, 5.4; N, 5.3. Found: C, 82.9; H, 5.8; N, 5.6.

Received: February 22, 2007
Revised: March 30, 2007
Published online: October 23, 2007

[1] a) C. W. Tang, S. A. Vanslyke, *Appl. Phys. Lett.* **1987**, *51*, 913. b) J. H. Burroughes, D. D. C. Bradley, A. R. Brown, R. N. Marks, K. Mackay, R. H. Friend, P. L. Burns, A. B. Holmes, *Nature* **1990**, *347*, 539. c) M. A. Baldo, D. F. O'Brien, Y. You, A. Shoustikov, S. Sibley, M. E. Thompson, S. R. Forrest, *Nature* **1998**, *395*, 151.

[2] a) M. A. Baldo, S. Lamansky, P. E. Burrows, M. E. Thompson, S. R. Forrest, *Appl. Phys. Lett.* **1999**, *75*, 4. b) E. Holder, B. M. W. Langeveld, U. S. Schubert, *Adv. Mater.* **2005**, *17*, 1109.

[3] a) Y. Su, H. Huang, C. Li, C. Chien, Y. Tao, P. Chou, S. Datta, R. Liu, *Adv. Mater.* **2003**, *15*, 884. b) C. Yang, C. Tai, I. Sun, *J. Mater. Chem.* **2004**, *14*, 947. c) Y. Song, S. Yeh, C. Chen, Y. Chi, C. Liu, J. Yu, Y. Hu, P. Chou, S. Peng, G. Lee, *Adv. Funct. Mater.* **2004**, *14*, 1221.

[4] S. C. Lo, E. B. Namdas, P. L. Burn, I. D. W. Samuel, *Macromolecules.* **2003**, *36*, 9721.

[5] a) J. P. J. Markham, I. D. W. Samuel, S. C. Lo, P. L. Burn, M. Weiter, H. Bassler, *J. Appl. Phys.* **2004**, *95*, 438. b) T. D. Anthopoulos, J. P. J. Markham, E. B. Namdas, J. R. Lawrence, I. D. W. Samuel, S. C. Lo, P. L. Burn, *Org. Electron.* **2003**, *4*, 71. c) E. B. Namdas, A. Ruseckas, I. D. W. Samuel, S. C. Lo, P. L. Burn, *J. Phys. Chem. B.* **2004**, *108*, 1570.

[6] T. Tsuzuki, N. Shirasawa, T. Suzuki, S. Tokito, *Jpn J. Appl. Phys.* **2005**, *44*, 4151.

[7] S. C. Lo, N. A. H. Male, J. P. J. Markham, S. W. Magennis, P. L. Burn, O. V. Salata, I. D. W. Samuel, *Adv. Mater.* **2002**, *14*, 975.

[8] T. D. Anthopoulos, J. P. J. Markham, E. B. Namdas, I. D. W. Samuel, S. C. Lo, P. L. Burn, *Appl. Phys. Lett.* **2003**, *82*, 4824.

[9] J. Ding, J. Gao, Y. Cheng, Z. Xie, L. Wang, D. Ma, X. Jing, F. Wang, *Adv. Funct. Mater.* **2006**, *16*, 575.

[10] T. D. Anthopoulos, M. J. Frampton, E. B. Namdas, P. L. Burn, I. D. W. Samuel, *Adv. Mater.* **2004**, *16*, 557.

[11] a) S. Lamansky, P. Djurovich, D. Murphy, F. Abdel-Razzaq, R. Kwong, I. Tsyba, M. Bortz, B. Mui, R. Bau, M. E. Thompson, *Inorg. Chem.* **2001**, *40*, 1704. b) F. Hwang, H. Chen, P. Chen, C. Liu, Y. Chi, C. Shu, F. Wu, P. Chou, S. Peng, G. Lee, *Inorg. Chem.* **2005**, *44*, 1344.

[12] A. Tsuboyama, H. Iwawaki, M. Furugori, T. Mukaide, J. Kamatani, S. Igawa, T. Moriyama, S. Miura, T. Takiguchi, S. Okada, M. Hoshino, K. Ueno, *J. Am. Chem. Soc.* **2003**, *125*, 12 971.

[13] J. Duan, P. Sun, C. Cheng, *Adv. Mater.* **2003**, *15*, 224.

[14] a) P. Coppo, E. A. Plummer, L. De Cola, *Chem. Commun.* **2004**, 1774. b) S. Lamansky, P. Djurovich, D. Murphy, F. Abdel-Razzaq, H. Lee, C. Adachi, P. E. Burrows, S. R. Forrest, M. E. Thompson, *J. Am. Chem. Soc.* **2001**, *123*, 4304.

[15] C. Yang, C. Tai, I. Sun, *J. Mater. Chem.* **2004**, *14*, 947.

[16] a) R. Hage, R. Prins, J. G. Haasnoot, J. Reedijk, J. G. Vos, *J. Chem. Soc. Dalton Trans.* **1987**, 1389. b) C. Chen, J. Shi, *Coord. Chem. Rev.* **1998**, *171*, 161.

[17] H. Doi, M. Kinoshita, K. Okumoto, Y. Shirota, *Chem. Mater.* **2003**, *15*, 1080.

[18] N. Miyaura, A. Suzuki, *Chem. Rev.* **1995**, *95*, 2457.

[19] B. Liang, C. Jiang, Z. Chen, X. Zhang, H. Shi, Y. Cao, *J. Mater. Chem.* **2006**, *16*, 1281.

[20] M. K. Nazeeruddin, R. Humphry-Baker, D. Berner, S. Rivier, L. Zuppiroli, M. Graetzel, *J. Am. Chem. Soc.* **2003**, *125*, 8790.

[21] A. B. Tamayo, B. D. Alleyne, P. I. Djurovich, S. Lamansky, I. Tsyba, N. N. Ho, R. Bau, M. E. Thompson, *J. Am. Chem. Soc.* **2003**, *125*, 7377.

[22] W. Wong, G. Zhou, X. Yu, H. Kwok, B. Tang, *Adv. Funct. Mater.* **2006**, *16*, 838.

[23] J. L. Bredas, R. Silbey, D. S. Boudreaux, R. R. Chance, *J. Am. Chem. Soc.* **1983**, *105*, 6555.

[24] A. P. Kulkarni, C. J. Tonzola, A. Babel, S. A. Jenekhe, *Chem. Mater.* **2004**, *16*, 4556.

[25] C. Jiang, W. Yang, J. Peng, S. Xiao, Y. Cao, *Adv. Mater.* **2004**, *16*, 537.

[26] a) P. A. Lane, L. C. Palilis, D. F. O'Brien, C. Giebeler, A. J. Cadby, D. G. Lidzey, A. J. Campbell, W. Blau, D. D. C. Bradley, *Phys. Rev. B: Condens. Matter Mater. Phys.* **2001**, *63*, 235 206. b) X. Gong, J. C. Ostrowski, D. Moses, G. C. Bazan, A. J. Heeger, *Adv. Funct. Mater.* **2003**, *13*, 439.

[27] H. B. Goodbrand, N. X. Hu, *J. Org. Chem.* **1999**, *64*, 670.